Brain networks modulated by subthalamic nucleus deep brain stimulation

Ettore A. Accolla,[1,2] **Maria Herrojo Ruiz,**[1,3] **Andreas Horn,**[1] **Gerd-Helge Schneider,**[4]
Tanja Schmitz-Hübsch,[1] **Bogdan Draganski**[5,6,]* **and Andrea A. Kühn**[1,7,8,9,]*

*These authors contributed equally to this work.

Deep brain stimulation of the subthalamic nucleus is an established treatment for the motor symptoms of Parkinson's disease. Given the frequent occurrence of stimulation-induced affective and cognitive adverse effects, a better understanding about the role of the subthalamic nucleus in non-motor functions is needed. The main goal of this study is to characterize anatomical circuits modulated by subthalamic deep brain stimulation, and infer about the inner organization of the nucleus in terms of motor and non-motor areas. Given its small size and anatomical intersubject variability, functional organization of the subthalamic nucleus is difficult to investigate *in vivo* with current methods. Here, we used local field potential recordings obtained from 10 patients with Parkinson's disease to identify a subthalamic area with an analogous electrophysiological signature, namely a predominant beta oscillatory activity. The spatial accuracy was improved by identifying a single contact per macroelectrode for its vicinity to the electrophysiological source of the beta oscillation. We then conducted whole brain probabilistic tractography seeding from the previously identified contacts, and further described connectivity modifications along the macroelectrode's main axis. The designated subthalamic 'beta' area projected predominantly to motor and premotor cortical regions additional to connections to limbic and associative areas. More ventral subthalamic areas showed predominant connectivity to medial temporal regions including amygdala and hippocampus. We interpret our findings as evidence for the convergence of different functional circuits within subthalamic nucleus' portions deemed to be appropriate as deep brain stimulation target to treat motor symptoms in Parkinson's disease. Potential clinical implications of our study are illustrated by an index case where deep brain stimulation of estimated predominant non-motor subthalamic nucleus induced hypomanic behaviour.

1 Department of Neurology, Charité University Medicine Berlin, Campus Virchow, 13353 Berlin, Germany
2 Neurology Unit, Medicine Department, HFR Cantonal Hospital and Faculty of Sciences, University of Fribourg, 1708 Fribourg, Switzerland
3 Department of Psychology, Goldsmiths, University of London, London SE14 6NW, UK
4 Department of Neurosurgery, Charité University Medicine Berlin, Campus Virchow, 13353 Berlin, Germany
5 LREN - Département des neurosciences cliniques, CHUV, Université de Lausanne, 1011 Lausanne, Switzerland
6 Max Planck Institute for Human Cognitive and Brain Science, 04103 Leipzig, Germany
7 Berlin School of Mind and Brain, Humboldt University, 10117 Berlin, Germany
8 NeuroCure Clinical Research Center, Charité - Universitätsmedizin Berlin, 10117 Berlin, Germany
9 DZNE, Berlin, Germany

Correspondence to: Dr Ettore Accolla,
Neurology Unit, Department of Medicine,
HFR – Hôpital Cantonal Fribourg and Fribourg University,
Chemin des Pensionnats 2-6, 1708 Fribourg,
Switzerland
E-mail: ettoreaccolla@gmail.com

Introduction

Deep brain stimulation (DBS) of the subthalamic nucleus (STN) in Parkinson's disease leads to effective reduction of motor symptoms and improvement of quality of life (Krack *et al.*, 2003; Schuepbach *et al.*, 2013). Despite its efficacy in ameliorating motor symptoms, DBS of the STN is also associated with affective, behavioural and cognitive adverse effects (Voon *et al.*, 2006; Castrioto *et al.*, 2014; Welter *et al.*, 2014). The most frequently observed symptoms include emotional instability (Krack *et al.*, 2001; Odekerken *et al.*, 2013) additional to induction of (hypo)manic episodes (Kulisevsky *et al.*, 2002; Mallet *et al.*, 2007; Ulla *et al.*, 2011; Chopra *et al.*, 2012; Welter *et al.*, 2014) and impulsivity changes (Frank *et al.*, 2007; Cavanagh *et al.*, 2011), alongside depression and apathy most probably due to medication reduction (Okun *et al.*, 2009; Thobois *et al.*, 2010; Witt *et al.*, 2012). Given that one of the main determinants of clinical outcome is the precise location of the macroelectrode (Castrioto *et al.*, 2014), a detailed knowledge of STN anatomy is particularly relevant for optimal target choice and DBS efficiency.

Although recently disputed (Alkemade and Forstmann, 2014; Lambert *et al.*, 2015), mounting evidence from anatomical, neurophysiological and clinical studies confirms the notion of a tripartite functional organization of the human STN (Krack *et al.*, 2001; Hamani *et al.*, 2004; Mallet *et al.*, 2007; Karachi *et al.*, 2009; York *et al.*, 2009). Despite the assumption of functional specialization, the putative segregated sensorimotor, associative and limbic territories show substantial areas of overlap (Haynes and Haber, 2013). The STN functional subregions can be distinguished with a certain degree of precision using neurophysiological markers, a procedure that is widely used in the clinical routine for electrode implantation (Rodriguez-Oroz *et al.*, 2001; Abosch *et al.*, 2002; Marceglia *et al.*, 2010; Kinfe and Vesper, 2013). In patients with Parkinson's disease, local field potential (LFP) recordings from the STN demonstrated enhanced oscillations in the beta band (13–30 Hz), which is substantially and consistently reduced after the intake of levodopa along with symptom improvement (Kühn *et al.*, 2006; Hammond *et al.*, 2007). Interestingly, neurons with predominant firing at frequencies within the beta range or those that are locked to oscillatory beta band activity are significantly more abundant in the dorso-lateral portion of the STN (Weinberger *et al.*, 2006; Trottenberg *et al.*, 2007; Zaidel *et al.*, 2010), a region that is part of the cortico-basal ganglia motor loop (Haynes and Haber, 2013). Beta activity could therefore be considered as the electrophysiological signature of the sensori-motor function within the dorso-lateral STN (Chen *et al.*, 2006; Trottenberg *et al.*, 2007; Zaidel *et al.*, 2010).

An inherent limitation when studying *in vivo* the anatomical and functional organization of the STN is due to the high level of interindividual variability (Richter *et al.*, 2004). Addressing this limitation, we combine neurophysiological recordings with brain imaging data from Parkinson's disease patients undergoing DBS of the STN. The main goal of the study was to obtain fine-grained topographical information about the STN functional subregions through characterization of its anatomical and functional connectivity patterns. To this aim, we used LFP recordings from DBS macroelectrodes within the STN in parallel with investigation of the anatomical connectivity of the very same DBS contacts based on probabilistic diffusion tractography. Finally, we analysed how connectivity values vary along the macroelectrode main axis. Based on the clinical observation of reduction of DBS-induced psychiatric symptoms when shifting the stimulation site dorsally (Welter *et al.*, 2014), we hypothesized that different patterns of connectivity to limbic cortical structures differentiate neighbouring contacts in the electrodes implanted in the STN of patients with Parkinson's disease.

Materials and methods

We acquired data from 10 idiopathic Parkinson's disease patients recruited at the Charité Movement Disorders clinic and scheduled for DBS based on clinical decision. Inclusion criteria were an established clinical diagnosis of idiopathic Parkinson's disease, a proven response to levodopa and the absence of other neurological or psychiatric diagnosis not related to Parkinson's disease. STN targeting and stereotactic surgery were performed according to a standard protocol as detailed previously (Kühn *et al.*, 2009).

All subjects gave informed written consent to the study, which was approved by the local Ethics committee. Demographic and available clinical information is summarized in Table 1. Levodopa equivalent daily dosage was calculated according to a recent systematic review (Tomlinson *et al.*, 2010).

Pre-surgery MRI

Before surgery, all patients underwent quantitative multi-parameter brain imaging and diffusion-weighted imaging on a 3 T whole-body MRI system (Magnetom TIM Trio, Siemens Healthcare) using a 32-channel radio frequency head receive coil and radio frequency body transmit coil. The quantitative MRI protocol consisted of 3D multi-echo FLASH datasets with predominantly proton density weighting (repetition time = 23.7 ms, flip angle $\alpha = 6°$), T_1-weighting (repetition time/α = 18.7 ms/20°), and magnetization transfer weighting

Table 1 Demographic and clinical information

Patient	1	2	3	4	5	6	7	8	9	10
Age	51	63	62	51	55	53	52	57	66	71
Gender	M	M	M	F	M	M	M	F	F	M
Disease duration (years)	6	11	8	14	8	10	15	13	12	11
Stimulating contacts (R L)	1 / 1	1 / 1	1 / 1	2-3 + / 2	3 / 3	3 / 3	1 / 1	3 / 3	3 / 3	1 / 1
Beta phase reversal OFF (R L)	2 / 2	(-) / 1	1 / (-)	1 / 2	1 / 2	(-) / 1	3 / 2	2 / (-)	2 / 2	3 / 1
UPDRS III preop. OFF	29	34	21	(n.a.)	34	42	50	36	24	30
UPDRS III preop. ON	3	14	12	(n.a.)	20	13	38	15	16.5	22
UPDRS III med OFF/ stim off	30	47	22	45	32	39	50	n.a.	n.a.	n.a.
UPDRS III med OFF/ stim on	8	12	14	8	16	14	28	n.a	n.a	n.a.
UPDRS III DBS improvement %	73.33	74.47	36.36	82.22	50.00	64.10	44.00	n.a	n.a	n.a
LEDD preop	402	1382	1580	675	1689	1552	875	1380	832	3395
LEDD reduction postop %	35.32	16.42	50.31	88.88	67.49	70	71.42	n.a.	18.02	77.94

Macroelectrode contacts are indicated as follows: R = Right, L = Left; contacts from most ventral to most dorsal 0-1-2-3; (-) indicates that a phase reversal could not be identified in the recordings. UPDRS = Unified Parkinson's Disease Rating Score, part III (range 0–108). M = males; F = females; n.a. = not available. LEDD = levodopa equivalent daily dose (according to Tomlinson et al., 2010).

(repetition time/α = 23.7 ms/6°) contrast according to the previously published protocol (Draganski et al., 2011; Weiskopf et al., 2013).

The diffusion-weighted imaging protocol was performed with the following parameters: echo time = 80 ms, repetition time 8300 ms, acquisition matrix 128 × 128 voxels, 74 axial slices, yielding voxel size of 1.7 × 1.7 × 1.7 mm, bandwidth = 2003 Hz/pixel, diffusion weighting at a high b = 1000 s/mm^2 along 60 directions and six reference volumes at zero b-value acquired one every 10th high b-value acquisition.

Post-surgery local field potential recordings

Patients were studied 2–6 days after DBS implantation with externalized DBS electrodes and prior to their connection to the stimulator device (Macroelectrode 3389, Medtronic).

Bipolar LFP activity was recorded from adjacent contact pairs (01, 12, 23) in each DBS electrode, where 0 is the most ventral and 3 is the most dorsal contact (R = right, L = left). Signals were amplified 50 000-fold and filtered at 0.5–250 Hz on a Digitimer D360 (Digitimer Ltd) and recorded through a 1401 A-D converter (Cambridge Electronic Design) onto a computer using Spike2 software (Cambridge Electronic Design). Signals were sampled at 1 kHz (except in Patient 4, where signals were sampled at 826 Hz) and monitored on-line.

In all patients, LFP recordings of 3–5 min duration were performed at rest (i) after overnight withdrawal of dopaminergic mediation (OFF); and (ii) 1 h after intake of 200 mg of levodopa or 1.5 times the patient-specific morning levodopa dose (ON). For the analysis of the LFP signals a segment of 180 s without muscle or ocular artefacts was selected for each patient from the OFF and ON LFP recordings.

Post-surgery MRI

Within 5 days after surgery, patients underwent brain MRI as part of the clinical protocol to confirm the planned localization of the electrodes. Dedicated T$_2$-weighted fast-spin echo sequences were acquired in a 1.5 T MRI machine (NT Intera; Philips Medical Systems), with the following

parameters: repetition time/echo time, 3500/138 ms; echo-train length, 8; excitations, 3; flip angle, 90°; section thickness, 2 mm; field of view, 260 mm (in-plane resolution 0.51 × 0.51 mm); matrix size, 384 interpolated to 512; total acquisition time, 10 min 41 s; Philips software Version 11.1 level 4. This protocol allowed us to respect the manufacturer specifications in terms of allowed specific absorbance ratio, which was not exceeding 0.1 W/kg.

Data analysis

LFP and neuroimaging data were processed and analysed in Matlab 7 (Mathworks, Sherborn, MA, USA). Image processing was performed with the freely available Statistical Parametric Mapping software (SPM8; Wellcome Trust Centre for Neuroimaging, London, UK, http://www.fil.ion.ucl.ac.uk/spm/software/), running under Matlab 7. Probabilistic diffusion tractography was performed with the FDT diffusion toolbox in the framework of FSL (Behrens et al., 2007).

Analysis of local field potential activity

The continuous LFP recordings of 180-s length were used for the LFP analyses described in this section.

The power spectral density (PSD, in μV^2/Hz) of the raw data was computed with the standard fast Fourier transform (Welch method, Hanning window of 1 s, 75% overlap) for each patient and medication condition separately. The power spectral density (measured power: P) was then normalized into decibels (dB) with the average power spectral density (reference power: P_0) within 105–195 Hz (excluding the 145–155 Hz range to avoid possible harmonics of the 50 Hz power line noise) to account for between-subjects variability:

$$PSD(dB) = 10 log_{10}\left(\frac{P}{P_0}\right) \qquad (1)$$

To confirm that the OFF state was associated with a larger beta-band (13–30 Hz) LFP activity (Priori et al., 2004; Kühn et al., 2006), we first tested for spectral power differences between the OFF and ON states within the 1–100 Hz range. In this analysis, we averaged for each patient the normalized
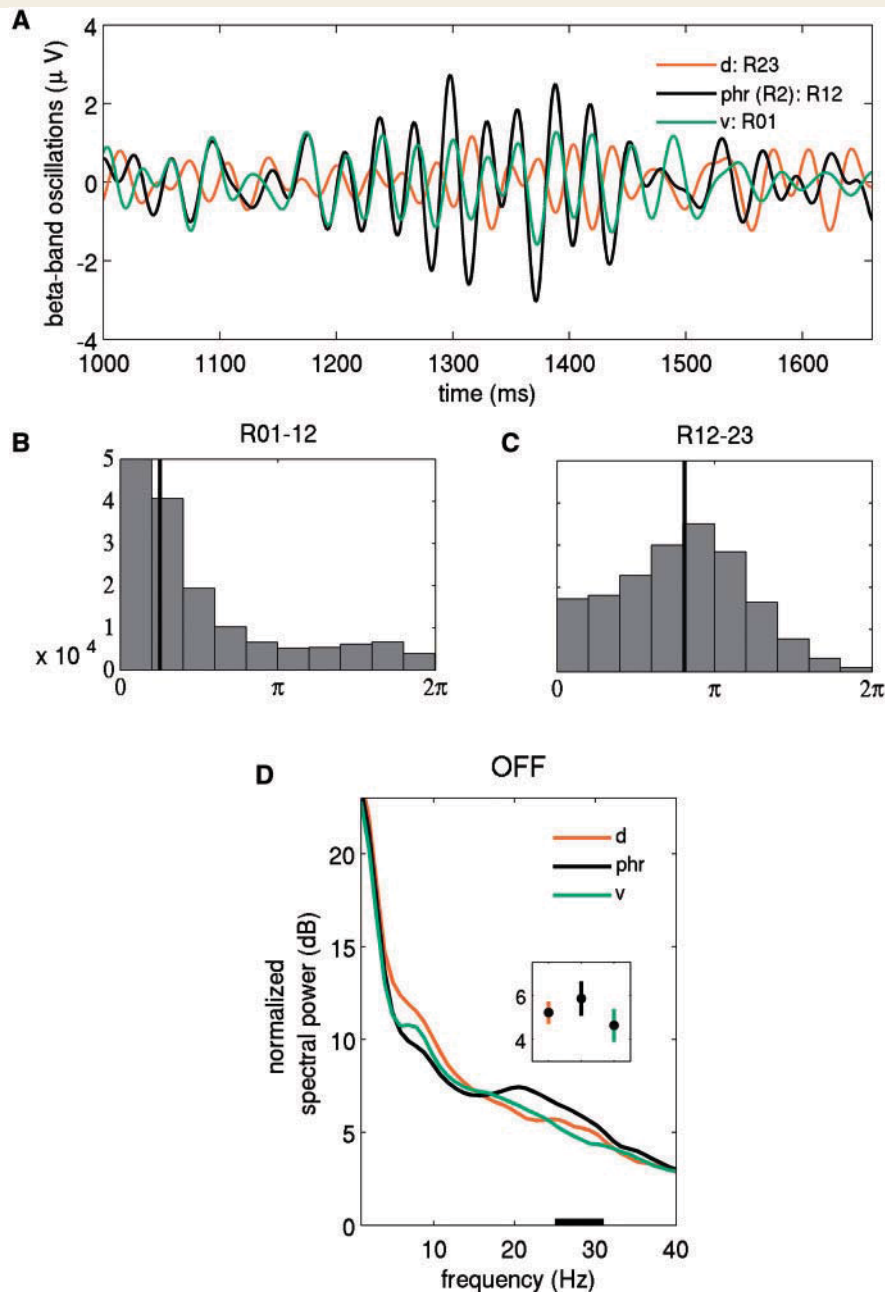
Figure 1 LFPs from STN-implanted macroelectrodes. (**A**) Representative time course of beta-band oscillatory activity in the right STN obtained from bipolar recordings in Patient 1. Note the phase reversal (phr) occurring between R12 and R23 (phase reversal at contact R2). For the power analysis, contact pair R12 was selected by convention (see main text) as the closest one to the source of beta activity (phase reversal). (**B**) Histogram depicting the difference phase values between signals recorded from contact pairs R01 and R12 in Patient 1. The maximum of the histogram is located at 0 radians (0°), indicating no phase reversal between both pairs. (**C**) Same for the difference phase values between signals recorded from contact pairs R12 and R23. In this case, the histogram attains its maximum value at π radians (180°), indicating the occurrence of phase reversal at contact R2. (**D**) Grand-average of the normalized spectral power OFF medication for the contact pair closest to the phase reversal of beta-band activity (potential source; phase reversal, in black), and for the dorsal (d, orange line) and ventral (v, green line) contact pairs. A significant effect of localization on the spectral power was obtained within 26–30 Hz (Kruskall-Wallis test, $P < P_{th}$ = 0.0208, after control of FDR). The inset shows the mean value and corresponding standard error of the mean (SEM) for the spectral power (d, phr, v) averaged within the range 26–30 Hz, in which the significant effect was found.

power spectral density across all contact pairs (R01, R12, R23, L01, L12, L23).

Next, to confine the local generator of the beta-band activity based on our bipolar LFP recordings, we used the analysis of phase reversal of oscillatory activity (Rodriguez-Oroz *et al.*, 2011; Fig. 1), which provides a more consistent spatial localization than the evaluation of the peak of activity in the spectral power. The occurrence of significant phase reversal

between two pairs of bipolar recordings (i.e. between 12 and 23) indicates that the source of the activity, although spatially distributed, lies closer to the contact shared by both bipolar recordings (e.g. contact 2 in the previous example. As each electrode has only four contacts, this analysis was limited to three pairs per side; Fig. 1A–C).

Phase reversal was analysed for neighbouring contact pairs in each STN, in the OFF condition. Prior to the phase reversal analysis, the LFP signals were band-pass filtered (finite impulse response filter) between 13–30 Hz to obtain the signal content in the beta frequency range. Then, we applied the Hilbert transform to extract the phase values $\varphi_i(t,f)$ for each band-passed filtered bipolar recording i, at time point t and within the frequency band f. Our criterion of phase reversal was based on the computation of the cosine of the phase of the resultant vector:

$$v = \frac{1}{N} \sum_{k=1}^{N} exp\left(i\left(\varphi_{jk} - \varphi_{ik}\right)\right) \quad (2)$$

where N is the signal length (N = 180 000 sampling points) and

$$\Delta\varphi_{ji,k} = \varphi_{jk} - \varphi_{ik} \quad (3)$$

is the phase difference between neighbouring signals i and j from bipolar recordings at sampling (time) point k. A phase reversal occurs when the resultant phase difference is within the range $(\pi/2, 3\pi/2)$ radians and is thus associated with a negative cosine value (Fig. 1C). When a phase difference lies within the range $(-\pi/2, \pi/2)$ radians, no phase reversal occurs and, correspondingly, a positive cosine value is obtained (Fig. 1B). The statistical evaluation of the phase reversal was performed following Rodriguez-Oroz et al. (2011), with the Rayleigh test of uniformity of angle by obtaining the significance value according to the expression:

$$exp\left(-Nv^2\right) \quad (4)$$

where

$$\nu = \|V\| \quad (5)$$

is the norm of the resultant vector v.

Following this procedure, we selected in each STN the contact where the phase reversal occurred (e.g. 1) and, in addition, the next one in the dorsal (e.g. 2) and ventral direction (e.g. 0) along the macroelectrode axis (if available; note that whenever the phase reversal was estimated to occur beyond contact 3, there was no dorsal contact available; and whenever the phase reversal was estimated to occur beyond contact 0, no ventral contact was available. These estimations were based on a tendency of the cosine towards more negative values, either in the $0 \rightarrow 1 \rightarrow 2 \rightarrow 3$ direction or in the opposite direction. However, these effects did not represent a true phase reversal). Beta-band phase reversal occurred within the STN for the majority of the nuclei ($n = 16/20$). A detailed list of the contacts at the phase reversal of beta LFP activity is provided in Table 1.

We then analysed the normalized spectral power with respect to the localization of the contact pairs (in relation to the beta-band phase reversal). The selection of contact pairs for this analysis was based on the occurrence of a significant phase reversal: for phase reversal at contact 1 or 2 (left or right STN), we selected contact pair 12 and 23, respectively, as the closest one to the phase reversal. The remaining contact pairs were defined as 'ventral' to phase reversal contact pair for the one caudal to the phase reversal contact pair, and 'dorsal' contact pair for the one rostral to the phase reversal contact pair (if available, see above). Note that the contact pairs choice in relation to phase reversal proximity (found for only one contact) is arbitrary, but this criterion was kept for consistency.

MRI data processing

The multi-parameter maps were only used for the purpose of non-linear registration to standardized space.

Magnetization transfer maps were first linearly registered to the diffusion space (using as a destination volume the first B0 diffusion acquisition) and then segmented according to the standard unified segmentation approach in the framework of SPM (Ashburner and Friston, 2005). Deformation fields from the previous step allowed for the inverse deformation of labelled probabilistic cortical atlases from Montreal Neurological Institute (MNI) into individual native diffusion space, as well as for the transformation of tractography results into the common space for further analysis (see below). For delineation and labelling of cortical areas we used a combination of freely available probabilistic atlases: the Juelich atlas for medial temporal areas (Eickhoff et al., 2005, including amygdala and hippocampus) and the Harvard-Oxford cortical atlas (Desikan et al., 2006) for the remaining areas.

Each group of 10 diffusion-weighted images b = 1000 s/mm^2 volumes was affine registered to the respective reference b = 0 (b0) volume, and then with the first b0 volume of the block acquisition. Diffusion vector directions were corrected accordingly with in-house Matlab code. Postoperative T$_2$ images were subsequently linearly co-registered with the average reference b0 volume, allowing for superposition of electrode artefacts on the diffusion native space. The accuracy of the procedure was visually inspected, and coordinates of the central voxel of contact artefact manually identified. From these coordinates, cube-shaped seed masks for tractography were built by expanding to all neighbouring voxels (total seed volume = 27 voxels). We used the recently implemented LEAD-DBS toolbox (Horn and Kühn, 2015) to estimate contacts coordinates in the MNI space, and their spatial localization with respect to the STN Morel atlas (Krauth et al., 2010). With the settings used, the toolbox allowed for subject-specific non-linear registration after segmentation of structural images (Supplementary Fig. 1).

Whole-brain unconstrained probabilistic tractography was performed in subject specific native space using the default settings in FSL bedpostx with the following parameters: 10 000 originating tracts per voxel, curvature 0.2, step length 0.5. Distributions of diffusion parameters were estimated at each voxel to model the directions of up to two tensors per voxel (Behrens et al., 2007). Through the option 'classification targets' we computed for each contact-surrounding seed the average number of tracts reaching each cortical target.

To maintain consistency across subjects, tractography was conducted seeding from contacts closest to the beta source (hereafter contacts 'B'), from the adjacent dorsal contact (contacts 'D') and the adjacent ventral contact (contacts 'V'). In the case of contact 'B' being assigned to the most dorsal contact (due to a trend towards a phase reversal beyond contact 3: 2/20 cases; Table 1), the adjacent connectivity profile was

excluded from analysis (contact 'D'). The STNs showing no phase reversal were excluded from this analysis (4/20 cases).

To reduce well-known biases affecting the probabilistic tractography method (Morris *et al.*, 2008), we excluded targets in close proximity to the implanted electrodes, i.e. the basal ganglia. Moreover, the cingulate cortex was also excluded, after demonstration of an important proximity bias: connectivity values were strongly affected by the vicinity of corpus callosum, so that it was not possible to reliably distinguish tracts directed to cingulate cortex from inter-hemispherical projections.

For each side, seed-to-target connectivity matrices were thresholded at 50 tracts, and the values were transformed using the natural logarithm. Values were normalized in each subject by dividing them by the maximum connectivity value. Cortical targets were considered for further analysis only if connected to at least 50% of contacts B or D or V.

Statistical analysis

Spectral power differences between the OFF and ON states within the 1–100 Hz range were tested by means of a non-parametric pair-wise permutation test (Good, 2005) across *n* subjects, with a total of 5000 random permutations. The difference in sample means was the test statistic. The *P*-values were computed as the frequencies that the replications of the test statistic had absolute values greater than or equal to the experimental difference. Statistical tests of the changes in spectral power were assessed at each frequency within 1–100 Hz.

The statistical assessment of a general effect of localization (ventral, beta-band phase reversal, dorsal) on the spectral power was performed by means of the non-parametric Kruskal–Wallis one-way ANOVA test. This test was assessed at each frequency bin between 13 and 30 Hz, to determine whether the effect of pair localization on the beta-band spectral power occurred in a specific sub-band or in the full beta band.

Differences in connectivity among contacts B, D and V were first tested with the non- parametric Kruskal–Wallis test. *Post hoc* analyses between D and B or between V and B contacts were performed by means of pairwise permutation tests.

In all statistical analyses, differences were considered significant if $P < 0.05$. Correction of the significance level due to multiple comparisons was performed by controlling the false discovery rate at level q = 0.05 by means of an adaptive two-stage linear step-up procedure (Benjamini and Yekutieli, 2001). The corrected threshold *P*-value obtained from this procedure, P_{th}, was used to reject all null hypotheses fulfilling the condition: *P*-value $< P_{th}$. Throughout the paper, P_{th} is given when multiple comparisons are performed (spectral power or connectivity analysis).

Results

Clinical data

All patients showed a good clinical response both to levodopa [mean improvement in Unified Parkinson's Disease Rating Scale (UPDRS) III score = $52 \pm 7\%$, available for 9/10 patients] and to DBS (mean improvement with DBS off versus on, medication OFF, available for 7/10

patients = $61 \pm 5\%$). Demographical and clinical information is summarized in Table 1. Two patients presented with mood disturbances after surgery (Patients 5 and 6). Patient 5 (male, 55 years old) developed hypomanic behaviour with uncontrolled money spending and high irritability (see below) 4 months after surgery. Patient 6 (male, 53 years old) also presented with transient hypomanic behaviour immediately after surgery. However, a retrospective diagnosis of a pre-existing bipolar disorder could be established based on new anamnestic information. Symptoms stabilized under withdrawal of selective serotonin reuptake inhibitors and treatment with valproic acid over a period of a few weeks, and no clear relation with STN stimulation could be identified.

Source localization of beta-band local field potential oscillations and spectral power analysis

The average normalized spectral power OFF medication, as compared to ON medication, exhibited significantly larger values in the lower beta range (13–20 Hz, $P < P_{th} = 0.031$, Supplementary Fig. 2). This outcome confirmed that there was a higher level of beta-band activity OFF medication, which was assessed further using the phase reversal analysis. We found a significant phase reversal of the beta-band STN oscillatory activity OFF medication for the majority of the patients, and typically in both STNs (16 nuclei of 20 in 10 patients, $P < 10^{-6}$, see Fig. 1A–C, and Table 1). In four STNs stemming from four different patients, no significant phase reversal could be found. For two of these nuclei, postoperative imaging showed a slight medial positioning of the macroelectrode (Patients 3 and 6). For all other patients postoperative imaging confirmed the optimal electrode placement with at least one contact of the macroelectrode within STN.

The contacts closer to the beta source (contacts B), after transformation of coordinates onto the standard MNI space, were localized in the dorso-lateral (sensorimotor) STN (average MNI coordinates in mm $\pm$ SEM: right: $x = 11.25 \pm 0.41$; $y = -12.62 \pm 0.90$; $z = -6.62 \pm 0.41$; left: $x = -11.00 \pm 0.59$; $y = -13.12 \pm 0.51$; $z = -6.87 \pm 0.61$; Fig. 2). Neighbouring contacts located above (dorsal, contacts D) the contact exhibiting the beta-band phase reversal were placed mainly outside the STN, while contacts below (ventral, contacts V) were still within the nucleus borders (Fig. 2).

The assessment of a general effect of contact pair localization (beta-band phase reversal, dorsal and ventral) on the normalized spectral power OFF medication, revealed a significant effect in the upper beta band within 26–30 Hz (Kruskal–Wallis test, $P < P_{th} = 0.0208$; Fig. 1D). This was due to consistently larger beta-band power values at the phase reversal contact pairs, relative to the ventral and dorsal contact pairs. Accordingly, the analysis of the normalized spectral power based on the phase reversal classification of contact pairs demonstrated a frequency-
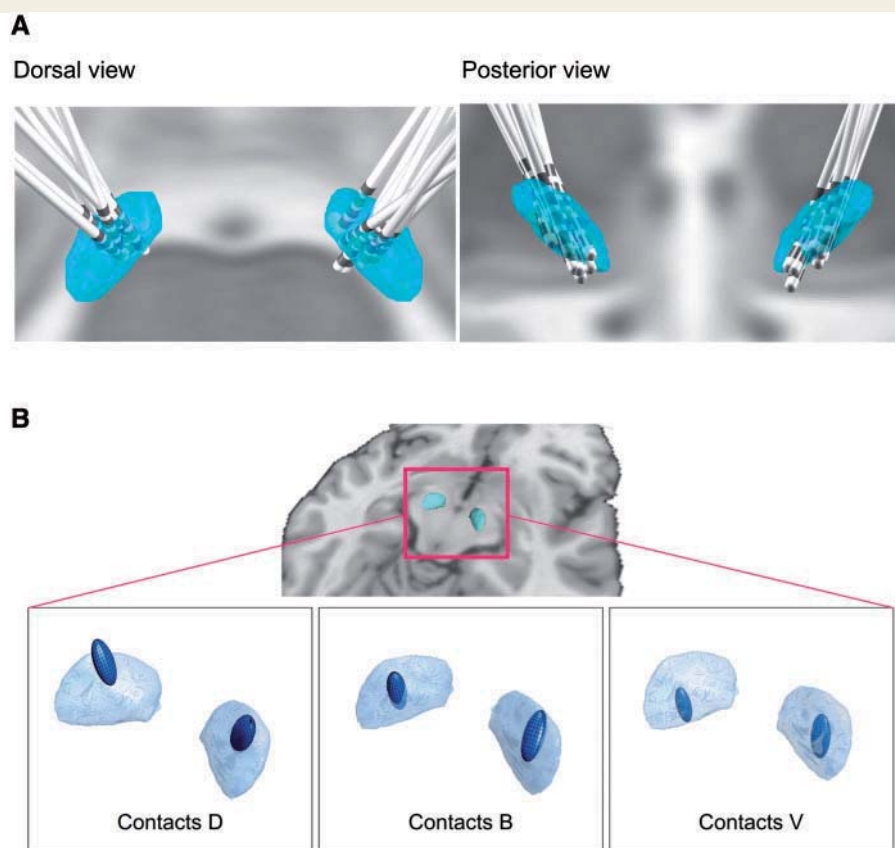
Figure 2 Localization of contacts in relation to the STN. Contacts coordinates were non-linearly registered to the MNI standard space, and superimposed to a STN 3D representation of the Morel stereotactic atlas (Krauth *et al.*, 2010). (**A**) 3D rendering of all leads postoperative position from a dorsal (*left*) and posterior (*right*) view. (**B**) Distribution model (coordinates average and covariance) of contacts in relation to the source of the beta oscillation. Contacts most close (contacts B, *middle*) lie in the dorso-lateral STN while neighbouring dorsal contacts (contacts D, *left*) are more frequently outside the nucleus. Contacts lying immediately beneath contacts B are closer to its inferior border (contacts V, *right*).

specific effect. By contrast, power analysis in the case of classification of contact pairs based on the peak of beta-band oscillatory activity revealed largely non-frequency specific (and non-significant) power modulations (Supplementary Fig. 3).

## Deep brain stimulation contacts: anatomical connectivity

Probabilistic tractography seeding from contacts B revealed a high connectivity to motor and premotor areas, and to a lesser extent to medial temporal and post-central structures (descriptive results in Fig. 3). In contrast, connectivity to amygdala, hippocampus and post-central gyrus were maximal from contacts V, and progressively reducing in the dorsal direction (Fig. 3). Connectivity to superior, middle and inferior frontal gyri, and supplementary motor cortex were highest in contacts D, intermediate in contacts B, and lowest in contacts V (Fig. 3).

The cortical areas that fulfilled both our criteria of (i) > 50 tract thresholding; and (ii) greater connectivity to at least 50% of either contacts B, D, and V included the frontal pole, superior, middle and inferior frontal gyrus, precentral gyrus, supplementary motor cortex, amygdala, hippocampus, superior parietal lobule, precuneus, and lateral occipital cortex. The non-parametric Kruskal–Wallis test revealed a main effect of contact localization (three levels: D, B, V) on the normalized connectivity to the amygdala, hippocampus, superior, middle and inferior frontal gyri, post-cental gyrus, supplementary motor cortex [$P < P_{th} = 0.01$, after control of false discovery rate (FDR) at level q = 0.05; Figs 3 and 4]. *Post hoc* analysis by means of permutation tests showed that contacts B had a significantly higher connectivity to the amygdala and smaller connectivity to the superior frontal gyrus than contacts D ($P < P_{th} = 0.01$). Compared to contacts V, contacts B had significantly smaller connectivity to the amygdala, whereas they had larger connectivity to the supplementary motor cortex, and the superior, middle and inferior frontal gyri ($P < P_{th} = 0.016$). Hence, in a dorso-ventral direction we described an increasing connectivity gradient to the amygdala, and a decreasing gradient of connectivity to supplementary motor cortex and the superior, middle and inferior frontal gyri.
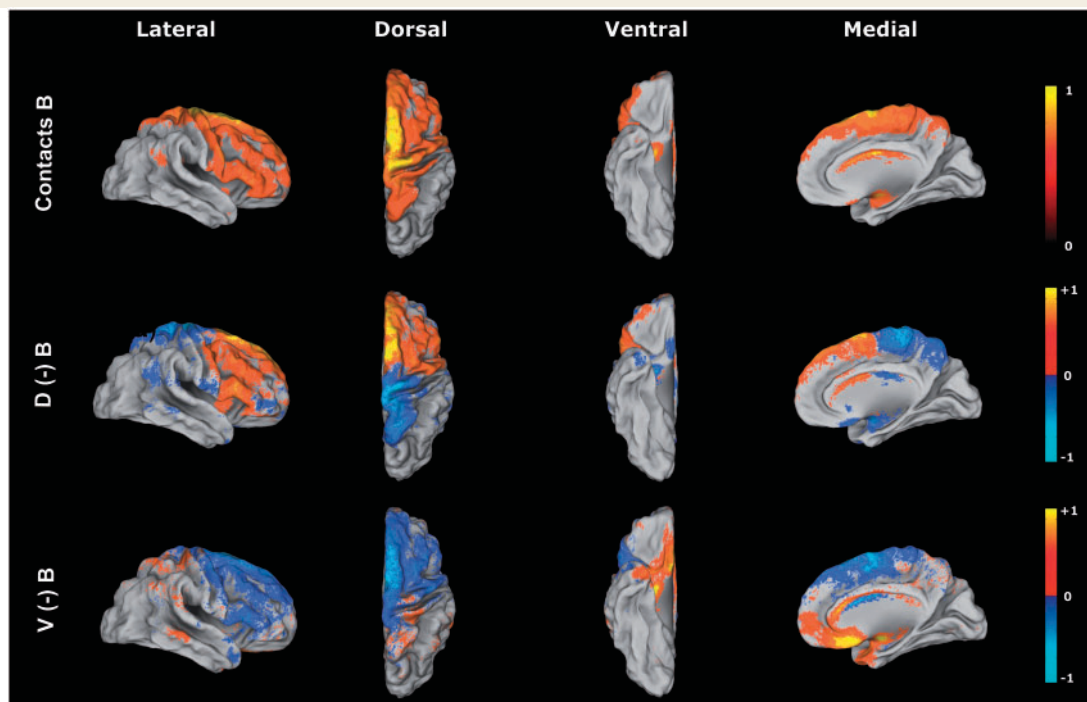
Figure 3 Probabilistic diffusion tractography from STN macroelectrode contacts. *Top row*: Connectivity profile of contacts closest to source of beta oscillations (contacts B). Regions with highest connectivity (yellow) include precentral gyrus and superior frontal gyrus. Lower connectivity values were found for prefrontal cortex and medial temporal regions. *Middle row*: Normalized difference of connectivity values: contacts dorsal to beta minus contacts closest to beta source [D(−)B]. *Bottom row:* Contacts ventral to beta minus contacts closest to beta source [V(−)B]. More dorsal contacts show higher connectivity to prefrontal associative regions, while most ventral contacts have higher connectivity to medial temporal and orbitofrontal regions.
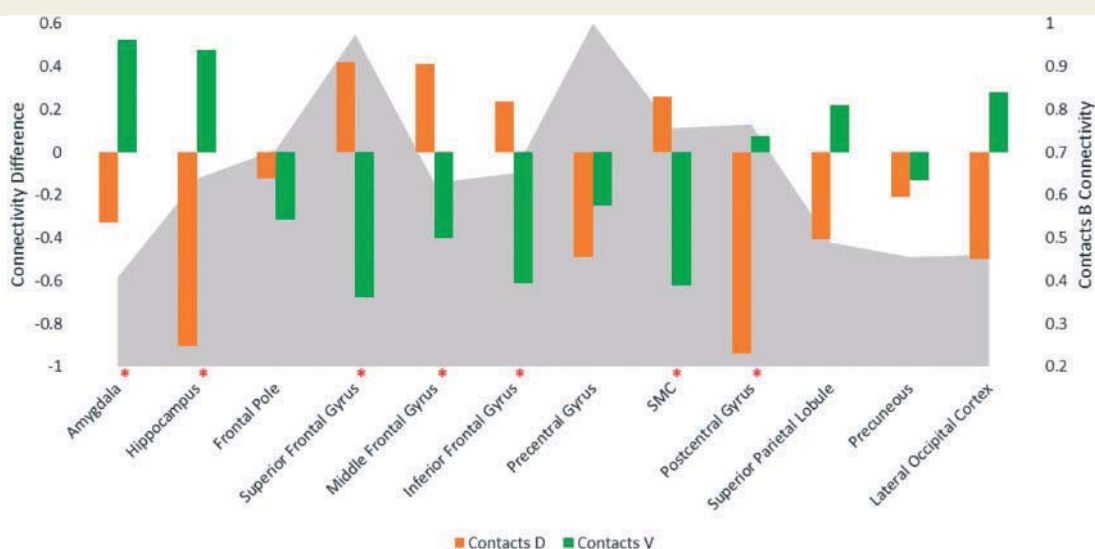
Figure 4 Kruskal–Wallis test showing a significant (asterisk) effect of localization for connectivity to cortical targets surviving threshold. For further details see 'Patients and methods' section. Columns represent normalized difference of connectivity values between (i) contacts dorsal to beta (D, orange) and contacts closest to beta source: D − source; and (ii) contacts ventral (V, green) to beta and contacts closest to beta source: V − source. Connectivity to amygdala and hippocampus increases towards more ventral contacts, whereas more dorsal contacts show increased connectivity to prefrontal cortex (superior, middle and inferior frontal gyrus) and supplementary motor cortex (SMC), and decreased connectivity to postcentral gyrus. Significance is set at $P < P_{th} = 0.01$, after control of false discovery rate at level q = 0.05. On the background, connectivity of beta contacts is represented by the shaded grey area (right *y*-axis).

Index case: clinical and imaging findings

Patient 5 (male, 54 years old at surgery) developed stimulation-induced hypomanic episodes. The patient underwent STN stimulation with no peri-operative complications and good motor response after activation of contacts 1R and 1L (second contact proceeding ventro-dorsally, right and left, respectively). For the same contacts, we observed the appearance of hemi-corporal sensory symptoms at 2.4 V amplitude bilaterally. Over the next few months, the positive effect on the motor symptoms waned progressively, prompting successive adaptations including shifting to the contacts above (2R and 2L). The pharmacological treatment was also optimized and included levodopa/carbidopa/entacapone and pramipexole. The total amount was 40% less than before surgery.

Six days after the last stimulation voltage increase to 2.5 V (right STN) and 2.7 V (left STN), 60 µs, 130 Hz, the patient complained of restlessness and irritability. His son reported irascible behaviour and episodes of uncontrolled, unnecessary money spending (mounting up to a car purchase). The psychiatric symptoms were almost completely resolved by reducing the intensity of the stimulation to 2.0 V and 2.1 V while the patient did not tolerate further reduction of the oral treatment. The lasting emotional irritability during in-patient care evolved further in a hypomanic state. The restlessness and logorrhoea could be prompted by increasing the stimulation voltage at contacts 2 bilaterally to rapidly disappear when the DBS was turned off. The psychiatric assessment was consistent with DBS-induced manic episodes given that the patient had no similar symptoms prior to surgery. After stimulation was shifted to most dorsal contacts (3R and 3L), there was a prompt optimal motor response associated with a subjective appeasing sensation. In the long-term observation there was a complete resolution of the psychiatric symptoms despite further increases in voltage up to 2.9 V in the right and 2.7 V in left STN.

The stereotactic localization according to the Morel STN atlas showed that the contacts eliciting hypomanic manifestations were positioned slightly anterior and ventral to the putative motor area, particularly in the left STN (Fig. 5A). The connectivity results in this patient confirmed the trend observed in the rest of the population (Fig. 5B). The tracts originating from the contacts 2 bilaterally were subtracted from those originating from contacts 3. Ventral contacts, eliciting manic manifestations (contacts 2R and 2L) had higher connectivity to medial temporal cortex, and lower to primary motor cortex as compared to dorsal contacts (contacts 3R and 3L). There was a certain asymmetry, with the left STN showing globally lower connectivity to prefrontal cortex. Clinical testing was not conducted separately for each side, so it was not possible to ascertain whether psychiatric side effects were caused predominantly by one of the two macroelectrodes.

Discussion

In our study we combine neurophysiological recordings with MRI to investigate *in vivo* subthalamic nucleus' functional organization. In the effort of overcoming the limitations of both methods, we gather evidence on the existence of overlapping functional subregions within the nucleus. Our results provide a neurobiological interpretation of the manifold clinical effects of DBS to further yield valuable information guiding clinical decision-making. These findings expand the current knowledge suggesting a rather complex and possibly subject-specific interplay between anatomical connectivity and neural activity patterns.

Sensory-motor subthalamic nucleus

We found that the target for DBS—the dorso-lateral STN—is characterized by beta oscillations and anatomical connections to motor cortical areas, suggesting a link between electrophysiological activity, connectivity, and function. Our neurophysiological findings confirm previous reports based on single unit recordings and LFP spectral analysis (Kühn et al., 2005; Weinberger et al., 2006; Trottenberg et al., 2007; Zaidel et al., 2010). The depicted anatomical network of the STN beta oscillatory region is compatible with the sensorimotor function previously attributed to the beta rhythm (Engel and Fries, 2010; Little and Brown, 2014). The most highly connected targets include sensorimotor areas—precentral, postcentral gyrus, supplementary motor cortex. This finding is consistent with the 'hyper-direct' pathway connecting primary motor areas with the dorso-lateral STN (Nambu et al., 1996; Whitmer et al., 2012; Haynes and Haber, 2013), and with the beta-coherence observed between STN and M1 (Marsden et al., 2001; Fogelson et al., 2006; Litvak et al., 2011).

The current knowledge about the generator of beta oscillations recorded from the STN is sparse; however, strong evidence indicates that cortical activity drives beta oscillations in the STN (Fogelson et al., 2006; Lalo et al., 2008; Litvak et al., 2011; Hirschmann et al., 2013). Although not statistically significant, we found that contacts closest to the beta source had highest connectivity to the precentral gyrus. This could represent the anatomical basis of the observed beta coherence among STN and precentral gyrus activity as recorded from subdural electrodes (Whitmer et al., 2012).

Besides confirming the known topography of the sensorimotor STN, we restrain from oversimplifying STNs functional organization. The demonstrated pattern of connectivity strongly suggests that STN areas involved in the origin of beta activity in Parkinson's disease project not only to sensorimotor areas, but also to regions involved in cognitive and emotional/behavioural functions: contacts B were also highly connected to prefrontal regions, including superior, middle and inferior frontal gyri; higher order sensory areas in the post-central gyrus, precuneus, superior parietal lobule additional to medial frontal and temporal
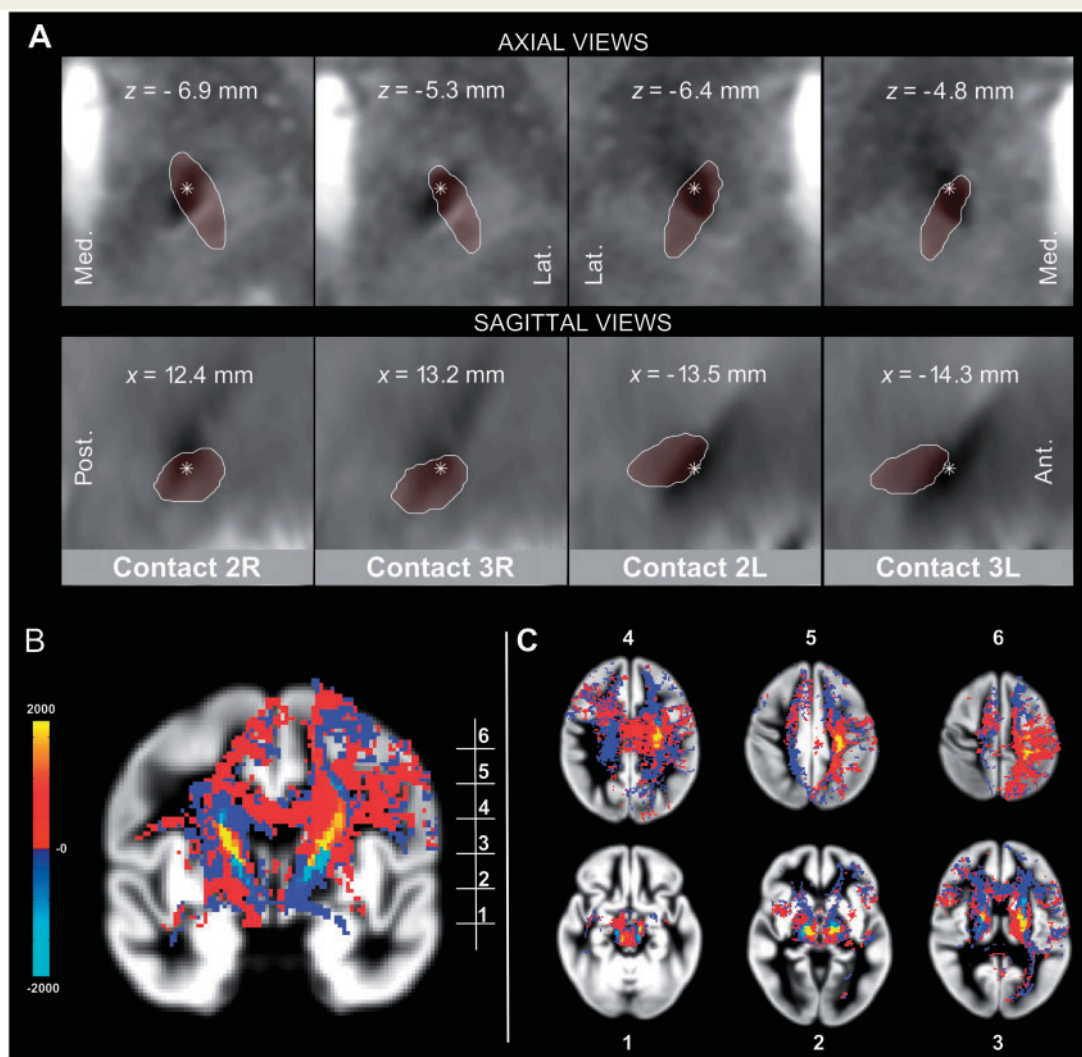
Figure 5 Imaging data of Patient 5. This subject had a significant motor improvement after stimulation from contacts 2 (right and left), but developed manic behaviour and restlessness. After shifting more dorsally (contacts 3 bilaterally) motor benefit was maintained, and psychiatric manifestations relieved. (**A**) MNI localization of stimulating contacts, superimposed to the Morel STN atlas (in purple, from Krauth *et al.,* 2010). *Top row*: axial view, with *z* coordinates specifying the section level (vertical axis). *Bottom row*: sagittal view, with *x* coordinates (right to left axis). Contacts eliciting hypomanic manifestations (2L and 2R) are located in a more anterior and ventral position within the nucleus. (**B**) Voxelwise, whole brain connectivity difference between contacts 2 and 3 (both sides computed separately) are shown (coronal view). In blue/light-blue voxels with higher connectivity to ventral contacts (contacts 2 versus contacts 3). In orange/red voxels with higher connectivity to dorsal contacts (contacts 3). Values represent the difference of number of tracts passing from each voxel. (**C**) Transversal sections at different *z* coordinates. Ventral contacts have higher connectivity to medial temporal structures, including amygdala, while more dorsal contacts have higher connectivity values to primary motor areas (particularly on the right side). Clinical effects were not tested separately for each side.

regions also showed high connectivity with 'beta' contacts. These results have to be interpreted with caution given major limitations in spatial resolution of MRI that we tried to overcome. However, we estimate that our careful beta source localization, high resolution DWI sequence (1.7 mm isotropic), and probabilistic tractography reached a sufficient reliability for inferring STN's functional organization. The notion of a tripartite STN—constituted by motor, associative and limbic functional subregions—is supported by consistent evidence (Krack *et al.*, 2001; Hamani *et al.*, 2004; Mallet *et al.*, 2007; Karachi *et al.*, 2009; York *et al.*, 2009). However, STN anatomo-functional subdivisions are not clear-cut as demonstrated by anatomical and neurophysiological evidence. Distribution of prefrontal projections to STN in the non-human primate (Haynes and Haber, 2013) and in humans as captured by recent imaging studies (Mallet *et al.*, 2007; Brunenberg *et al.*, 2012; Lambert *et al.*, 2012; Accolla *et al.*, 2014) show convergence and multiple areas of overlap. STN subareas are also not clearly segregated from a neurophysiological point of view, as firing pattern modifications secondary to sensory-motor tasks have been observed in regions with no prominent beta activity (Zaidel *et al.*, 2010). Given these premises, our data further support that (i) beta oscillations are not restricted to

a 'motor' STN area; and (ii) that the 'motor' STN is not connected exclusively with motor cortical areas. We here show that where the electrophysiological source of beta activity is found, motor connectivity is predominant, but not exclusive. We conclude that beta oscillations have a main but not exclusive motor significance, and that STN might be organized following a topographical specialization by which predominant function at each location is constantly informed by other circuits' activity.

Subthalamic nucleus connectivity to limbic cortical areas

Comparison of neighbouring contacts revealed a significantly higher connectivity of ventral STN to limbic targets—medial temporal structures including hippocampus and amygdala. This principle of organization was also observed at the single subject level in a patient with DBS induced hypomanic manifestations. The involvement of amygdala and hippocampus in manic states—mostly investigated in the context of bipolar disorder—is well documented, with reported volume differences among patients and healthy subjects (Schneider *et al.*, 2012), and increased blood oxygen level-dependant functional MRI signal in response to affective faces during mania (Altshuler *et al.*, 2005; Malhi *et al.*, 2007; Strakowski *et al.*, 2012). In light of our findings, we provide a new interpretation of the previous report about STN-DBS induced decrease in regional cerebral blood flow, observed in the left medial and inferior temporal cortex in patients developing hypomaniac behaviour after stimulation (Ulla *et al.*, 2011). The presumption here is that STN-DBS induces hypomanic manifestations by modulating STNs impact on medial temporal lobe structures through inhibition of predominantly excitatory projections. Along these lines, in our index case we could not confirm the supposition that direct stimulation of substantia nigra structures is eliciting hypomanic symptoms (Ulla *et al.*, 2011) or acute depressive state (Bejjani *et al.*, 1999) as described previously. Altogether, our findings provide a plausible anatomical substrate for the occurrence of (hypo)manic states following STN DBS, and a rationale for improvement observed when shifting stimulation dorsally.

Methodological considerations

Our approach to differentiate STN contact pairs based on the proximity to the beta-band phase reversal aimed at increasing spatial resolution, and strengthens the validity of our conclusions. The alternative approach, based solely on maximum spectral power, was not frequency-specific (Supplementary Fig. 3). Rather, this approach revealed that the contact pair with maximum power in the beta range also exhibited maximum power in neighbouring frequency ranges, therefore suggesting a generally larger signal-to-noise ratio in these contacts but not a specific contact localization in the proximity of the generator of beta oscillations. With this respect, the phase reversal analysis provides a higher accuracy for spatial localization of oscillatory activity in a specific frequency range (Rodriguez-Oroz *et al.*, 2011).

One limitation of the beta source localization lies in the few available contact pairs per STN: four contacts amounting to three contact pairs. A larger number of contact pairs per STN could lead to a more accurate spatial localization of the beta oscillations, although it should also be noted that the beta-band activity pattern is not expected to be localized to a single focal point within the STN but may rather be spatially distributed across the dorso-lateral STN. An additional limitation that affects exclusively the power analysis is that it was necessary to set a criterion upon which to select the contact 'pair' closest to the phase reversal. That is, if a phase reversal was found between contact pairs 01 and 12, there was no ambiguity with regard to which 'contact' was closest to the phase reversal (here contact 1), but it was indeed necessary to decide which contact pair from the two containing the phase-reversal contact (1) should be selected for power analysis. Importantly, however, the connectivity analysis was not affected by this ambiguity.

In conclusion, our study expands the knowledge of STN anatomy and describes anatomical networks potentially modulated by DBS. We failed to address more specific clinical questions due to the retrospective nature of clinical data. We nevertheless here demonstrate the advantages of merging clinical, neurophysiological and neuroimaging data in investigating specific neuro-scientific questions relevant for medical purposes. We propose that future strategies for improving DBS outcome should focus beyond the schematic tripartite principle of organization, to target individually the optimal STN stimulation site.

Funding

Supplementary material

Supplementary material is available at *Brain* online.

References

Abosch A, Hutchison WD, Saint-Cyr JA, Dostrovsky JO, Lozano AM. Movement-related neurons of the subthalamic nucleus in patients with Parkinson disease. J Neurosurg 2002; 97: 1167–72.

Accolla EA, Dukart J, Helms G, Weiskopf N, Kherif F, Lutti A, et al. Brain tissue properties differentiate between motor and limbic basal ganglia circuits. Hum Brain Mapp 2014; 35: 5083–92

Alkemade A, Forstmann BU. Do we need to revise the tripartite subdivision hypothesis of the human subthalamic nucleus (STN)? Neuroimage 2014; 95: 326–9.

Altshuler L, Bookheimer S, Proenza MA, Townsend J, Sabb F, Firestine A, et al. Increased amygdala activation during mania: a functional magnetic resonance imaging study. Am J Psychiatry 2005; 162: 1211–13.

Ashburner J, Friston KJ. Unified segmentation. Neuroimage 2005; 26: 839–51.

Behrens TEJ, Berg HJ, Jbabdi S, Rushworth MFS, Woolrich MW. Probabilistic diffusion tractography with multiple fibre orientations: what can we gain? Neuroimage 2007; 34: 144–55.

Bejjani BP, Damier P, Arnulf I, Thivard L, Bonnet AM, Dormont D, et al. Transient acute depression induced by high-frequency deep brain stimulation. N Engl J Med 1999; 340: 1476–80.

Benjamini Y, Yekutieli D. The control of the false discovery rate in multiple testing under dependency. Ann Stat 2001; 29: 1165–88.

Brunenberg EJL, Moeskops P, Backes WH, Pollo C, Cammoun L, Vilanova A, et al. Structural and resting state functional connectivity of the subthalamic nucleus: identification of motor STN parts and the hyperdirect pathway. PloS One 2012; 7: e39061.

Castrioto A, Lhommée E, Moro E, Krack P. Mood and behavioural effects of subthalamic stimulation in Parkinson's disease. Lancet Neurol 2014; 13: 287–305.

Cavanagh JF, Wiecki TV, Cohen MX, Figueroa CM, Samanta J, Sherman SJ, et al. Subthalamic nucleus stimulation reverses mediofrontal influence over decision threshold. Nat Neurosci 2011; 14: 1462–67.

Chen CC, Pogosyan A, Zrinzo LU, Tisch S, Limousin P, Ashkan K, et al. Intra-operative recordings of local field potentials can help localize the subthalamic nucleus in Parkinson's disease surgery. Exp Neurol 2006; 198: 214–21.

Chopra A, Tye SJ, Lee KH, Sampson S, Matsumoto J, Adams A, et al. Underlying neurobiology and clinical correlates of mania status after subthalamic nucleus deep brain stimulation in Parkinson's disease: a review of the literature. J Neuropsychiatry Clin Neurosci 2012; 24: 102–10.

Desikan RS, Ségonne F, Fischl B, Quinn BT, Dickerson BC, Blacker D, et al. An automated labeling system for subdividing the human cerebral cortex on MRI scans into gyral based regions of interest. Neuroimage 2006; 31: 968–80.

Draganski B, Ashburner J, Hutton C, Kherif F, Frackowiak RSJ, Helms G, et al. Regional specificity of MRI contrast parameter changes in normal ageing revealed by voxel-based quantification (VBQ). Neuroimage 2011; 55: 1423–34.

Eickhoff SB, Stephan KE, Mohlberg H, Grefkes C, Fink GR, Amunts K, et al. A new SPM toolbox for combining probabilistic cytoarchitectonic maps and functional imaging data. Neuroimage 2005; 25: 1325–35.

Engel AK, Fries P. Beta-band oscillations—signalling the status quo? Curr Opin Neurobiol 2010; 20: 156–65.

Fogelson N, Williams D, Tijssen M, Bruggen G van, Speelman H, Brown P. Different functional loops between cerebral cortex and the subthalmic area in Parkinson's disease. Cereb Cortex 2006; 16: 64–75.

Frank MJ, Samanta J, Moustafa AA, Sherman SJ. Hold your horses: impulsivity, deep brain stimulation, and medication in Parkinsonism. Science 2007; 318: 1309–12.

Good PH. Permutation, parametric and bootstrap tests of hypotheses. In: Springer series in statistics. New York: Springer; 2005.

Hamani C, Saint-Cyr JA, Fraser J, Kaplitt M, Lozano AM. The subthalamic nucleus in the context of movement disorders. Brain 2004; 127: 4–20.

Hammond C, Bergman H, Brown P. Pathological synchronization in Parkinson's disease: networks, models and treatments. Trends Neurosci 2007; 30: 357–64.

Haynes WIA, Haber SN. The organization of prefrontal-subthalamic inputs in primates provides an anatomical substrate for both functional specificity and integration: implications for basal ganglia models and deep brain stimulation. J Neurosci 2013; 33: 4804–14.

Hirschmann J, Özkurt TE, Butz M, Homburger M, Elben S, Hartmann CJ, et al. Differential modulation of STN-cortical and cortico-muscular coherence by movement and levodopa in Parkinson's disease. Neuroimage 2013; 68: 203–13.

Horn A, Kühn AA. Lead-DBS: a toolbox for deep brain stimulation electrode localizations and visualizations. Neuroimage 2015; 107: 127–35.

Karachi C, Grabli D, Baup N, Mounayar S, Tandé D, François C, et al. Dysfunction of the subthalamic nucleus induces behavioral and movement disorders in monkeys. Mov Disord 2009; 24: 1183–92.

Kinfe TM, Vesper J. The impact of multichannel microelectrode recording (MER) in deep brain stimulation of the basal ganglia. Acta Neurochir Suppl 2013; 117: 27–33.

Krack P, Batir A, Van Blercom N, Chabardes S, Fraix V, Ardouin C, et al. Five-year follow-up of bilateral stimulation of the subthalamic nucleus in advanced Parkinson's disease. N Engl J Med 2003; 349: 1925–34.

Krack P, Kumar R, Ardouin C, Dowsey PL, McVicker JM, Benabid A-L, et al. Mirthful laughter induced by subthalamic nucleus stimulation. Mov Disord 2001; 16: 867–75.

Krauth A, Blanc R, Poveda A, Jeanmonod D, Morel A, Székely G. A mean three-dimensional atlas of the human thalamus: generation from multiple histological data. Neuroimage 2010; 49: 2053–62.

Kühn AA, Trottenberg T, Kivi A, Kupsch A, Schneider G-H, Brown P. The relationship between local field potential and neuronal discharge in the subthalamic nucleus of patients with Parkinson's disease. Exp Neurol 2005; 194: 212–20.

Kühn AA, Kupsch A, Schneider G-H, Brown P. Reduction in subthalamic 8-35 Hz oscillatory activity correlates with clinical improvement in Parkinson's disease. Eur J Neurosci 2006; 23: 1956–60.

Kühn AA, Tsui A, Aziz T, Ray N, Brücke C, Kupsch A, et al. Pathological synchronisation in the subthalamic nucleus of patients with Parkinson's disease relates to both bradykinesia and rigidity. Exp Neurol 2009; 215: 380–87.

Kulisevsky J, Berthier ML, Gironell A, Pascual-Sedano B, Molet J, Parés P. Mania following deep brain stimulation for Parkinson's disease. Neurology 2002; 59: 1421–24.

Lalo E, Thobois S, Sharott A, Polo G, Mertens P, Pogosyan A, et al. Patterns of bidirectional communication between cortex and basal ganglia during movement in patients with Parkinson disease. J Neurosci 2008; 28: 3008–16.

Lambert C, Zrinzo L, Nagy Z, Lutti A, Hariz M, Foltynie T, et al. Confirmation of functional zones within the human subthalamic nucleus: patterns of connectivity and sub-parcellation using diffusion weighted imaging. Neuroimage 2012; 60: 83–94.

Lambert C, Zrinzo L, Nagy Z, Lutti A, Hariz M, Foltynie T, et al. Do we need to revise the tripartite subdivision hypothesis of the human subthalamic nucleus (STN)? Response to Alkemade and Forstmann. Neuroimage 2015; 110: 1–2.

Little S, Brown P. The functional role of beta oscillations in Parkinson's disease. Parkinsonism Relat Disord 2014; 20 (Suppl 1): S44–48.

Litvak V, Jha A, Eusebio A, Oostenveld R, Foltynie T, Limousin P, et al. Resting oscillatory cortico-subthalamic connectivity in patients with Parkinson's disease. Brain J Neurol 2011; 134: 359–74.

Malhi GS, Lagopoulos J, Sachdev PS, Ivanovski B, Shnier R, Ketter T. Is a lack of disgust something to fear? A functional magnetic resonance imaging facial emotion recognition study in euthymic bipolar disorder patients. Bipolar Disord 2007; 9: 345–57.

Mallet L, Schüpbach M, N'Diaye K, Remy P, Bardinet E, Czernecki V, et al. Stimulation of subterritories of the subthalamic nucleus reveals its role in the integration of the emotional and motor aspects of behavior. Proc Natl Acad Sci USA 2007; 104: 10661–6.

Marceglia S, Mrakic-Sposta S, Tommasi G, Bartolomei L, Foresti C, Valzania F, et al. Multicenter study report: electrophysiological monitoring procedures for subthalamic deep brain stimulation surgery in Parkinson's disease. Neurol Sci 2010; 31: 449–57.

Marsden J, Limousin-Dowsey P, Fraix V, Pollak P, Odin P, Brown P. Intermuscular coherence in Parkinson's disease: effects of subthalamic nucleus stimulation. Neuroreport 2001; 12: 1113–17.

Morris DM, Embleton KV, Parker GJM. Probabilistic fibre tracking: differentiation of connections from chance events. Neuroimage 2008; 42: 1329–39.

Nambu A, Takada M, Inase M, Tokuno H. Dual somatotopical representations in the primate subthalamic nucleus: evidence for ordered but reversed body-map transformations from the primary motor cortex and the supplementary motor area. J Neurosci 1996; 16: 2671–83.

Odekerken VJ, van Laar T, Staal MJ, Mosch A, Hoffmann CF, Nijssen PC, et al. Subthalamic nucleus versus globus pallidus bilateral deep brain stimulation for advanced Parkinson's disease (NSTAPS study): a randomised controlled trial. Lancet Neurol 2013; 12: 37–44.

Okun MS, Fernandez HH, Wu SS, Kirsch-Darrow L, Bowers D, Bova F, et al. Cognition and mood in Parkinson's disease in subthalamic nucleus versus globus pallidus interna deep brain stimulation: the COMPARE trial. Ann Neurol 2009; 65: 586–95.

Priori A, Foffani G, Pesenti A, Tamma F, Bianchi AM, Pellegrini M, et al. Rhythm-specific pharmacological modulation of subthalamic activity in Parkinson's disease. Exp Neurol 2004; 189: 369–79.

Richter EO, Hoque T, Halliday W, Lozano AM, Saint-Cyr JA. Determining the position and size of the subthalamic nucleus based on magnetic resonance imaging results in patients with advanced Parkinson disease. J Neurosurg 2004; 100: 541–46.

Rodriguez-Oroz MC, López-Azcárate J, Garcia-Garcia D, Alegre M, Toledo J, Valencia M, et al. Involvement of the subthalamic nucleus in impulse control disorders associated with Parkinson's disease. Brain 2011; 134: 36–49.

Rodriguez-Oroz MC, Rodriguez M, Guridi J, Mewes K, Chockkman V, Vitek J, et al. The subthalamic nucleus in Parkinson's disease: somatotopic organization and physiological characteristics. Brain 2001; 124: 1777–90.

Schneider MR, DelBello MP, McNamara RK, Strakowski SM, Adler CM. Neuroprogression in bipolar disorder. Bipolar Disord 2012; 14: 356–74.

Schuepbach WMM, Rau J, Knudsen K, Volkmann J, Krack P, Timmermann L, et al. Neurostimulation for Parkinson's disease with early motor complications. N Engl J Med 2013; 368: 610–22.

Strakowski SM, Adler CM, Almeida J, Altshuler LL, Blumberg HP, Chang KD, et al. The functional neuroanatomy of bipolar disorder: a consensus model. Bipolar Disord 2012; 14: 313–25.

Thobois S, Ardouin C, Lhommée E, Klinger H, Lagrange C, Xie J, et al. Non-motor dopamine withdrawal syndrome after surgery for Parkinson's disease: predictors and underlying mesolimbic denervation. Brain 2010; 133: 1111–27.

Tomlinson CL, Stowe R, Patel S, Rick C, Gray R, Clarke CE. Systematic review of levodopa dose equivalency reporting in Parkinson's disease. Mov Disord 2010; 25: 2649–53.

Trottenberg T, Kupsch A, Schneider G-H, Brown P, Kühn AA. Frequency-dependent distribution of local field potential activity within the subthalamic nucleus in Parkinson's disease. Exp Neurol 2007; 205: 287–91.

Ulla M, Thobois S, Llorca P-M, Derost P, Lemaire J-J, Chereau-Boudet I, et al. Contact dependent reproducible hypomania induced by deep brain stimulation in Parkinson's disease: clinical, anatomical and functional imaging study. J Neurol Neurosurg Psychiatry 2011; 82: 607–14.

Voon V, Kubu C, Krack P, Houeto J-L, Tröster AI. Deep brain stimulation: neuropsychological and neuropsychiatric issues. Mov Disord 2006; 21 (Suppl 14): S305–27.

Weinberger M, Mahant N, Hutchison WD, Lozano AM, Moro E, Hodaie M, et al. Beta oscillatory activity in the subthalamic nucleus and its relation to dopaminergic response in Parkinson's disease. J Neurophysiol 2006; 96: 3248–56.

Weiskopf N, Suckling J, Williams G, Correia MM, Inkster B, Tait R, et al. Quantitative multi-parameter mapping of R1, PD*, MT and R2* at 3T: a multi-center validation. Front Neurosci 2013; 7: 95.

Welter M-L, Schüpbach M, Czernecki V, Karachi C, Fernandez-Vidal S, Golmard J-L, et al. Optimal target localization for subthalamic stimulation in patients with Parkinson disease. Neurology 2014; 82: 1352–61.

Whitmer D, de Solages C, Hill BC, Yu H, Henderson JM, Bronte-Stewart H. High frequency deep brain stimulation attenuates subthalamic and cortical rhythms in Parkinson's disease. Front Hum Neurosci 2012; 6: 155.

Witt K, Daniels C, Volkmann J. Factors associated with neuropsychiatric side effects after STN-DBS in Parkinson's disease. Parkinsonism Relat Disord 2012; 18 (Suppl 1): S168: 70.

York MK, Wilde EA, Simpson R, Jankovic J. Relationship between neuropsychological outcome and DBS surgical trajectory and electrode location. J Neurol Sci 2009; 287: 159–71.

Zaidel A, Spivak A, Grieb B, Bergman H, Israel Z. Subthalamic span of β oscillations predicts deep brain stimulation efficacy for patients with Parkinson's disease. Brain 2010; 133: 2007–21.